Alanis Ruiz, C., van Hooff, T., Blocken, B., and van Heijst, G.J.F. (2021). Air curtain performance: Introducing the adapted separation efficiency. *Building and Environment 188*: Article nr. 107468.

https://doi.org/10.1016/j.buildenv.2020.107468

AIR CURTAIN PERFORMANCE: INTRODUCING THE ADAPTED SEPARATION EFFICIENCY

Claudio Alanis Ruiz[1,*], Twan van Hooff[1,2], Bert Blocken[2,1], GertJan van Heijst[3]

[1]Building Physics and Sustainable Design Section, Department of Civil Engineering, KU Leuven, Belgium

[2]Building Physics and Services, Department of the Built Environment, Eindhoven University of Technology, the Netherlands

[3]Turbulence and Vortex Dynamics, Department of Applied Physics, Eindhoven University of Technology, the Netherlands

[*]*Corresponding email: claudio.alanisruiz@kuleuven.be; corresponding postal address: Kasteelpark Arenberg 40, P.O. Box 2447, 3001 Leuven, Belgium*

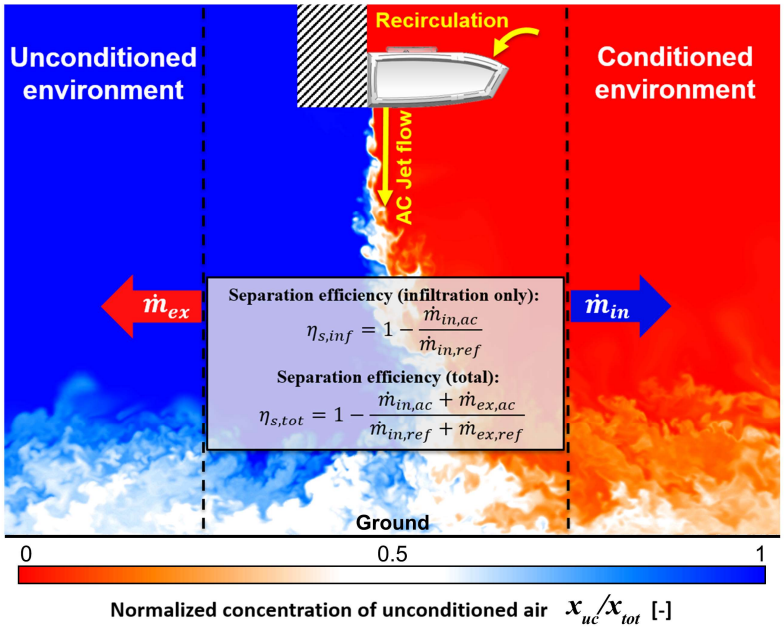

- A new indicator to evaluate air-curtain (AC) performance is proposed.
- The proposed indicator enables universal AC performance assessment.
- Its use is demonstrated in a case study consisting of representative AC systems.
- The case study is conducted by means of CFD employing validated LES models.

AIR CURTAIN PERFORMANCE: INTRODUCING THE ADAPTED SEPARATION EFFICIENCY

Claudio Alanis Ruiz[1,*], Twan van Hooff[1,2], Bert Blocken[2,1], GertJan van Heijst[3]

[1]Building Physics and Sustainable Design Section, Department of Civil Engineering, KU Leuven, Belgium

[2]Building Physics and Services, Department of the Built Environment, Eindhoven University of Technology, the Netherlands

[3]Turbulence and Vortex Dynamics, Department of Applied Physics, Eindhoven University of Technology, the Netherlands

[*]*Corresponding email: claudio.alanisruiz@kuleuven.be; corresponding postal address: Kasteelpark Arenberg 40, P.O. Box 2447, 3001 Leuven, Belgium*

Abstract:

Air curtains (ACs) are plane turbulent impinging jets that are used to separate two environments in terms of heat and mass transfer while still allowing traffic between these environments. The many applications of ACs across a wide variety of industries makes the evaluation of their performance an important but difficult task. The aim of this paper is to introduce a performance indicator, called the adapted separation efficiency, that is suitable for different types of systems that may involve different AC configurations (downward blowing, upward blowing, lateral blowing, multiple jets, etc.) at multiple scales, different transported quantities (heat, water vapor, particles, gases, etc.) subjected to various transport mechanisms (advection, molecular and turbulent diffusion) and varying environmental conditions (gradients in environmental pressure and/or density). It is defined using a conventional efficiency formula. The principle of this performance indicator is illustrated with a generic case study where the performance is evaluated for two basic AC configurations involving cross-jet pressure and density gradients, as well as different jet momentum fluxes. The case study is conducted based on computational fluid dynamics employing validated large eddy simulations.

Keywords: air curtain, separation efficiency, infiltration, computational fluid dynamics (CFD), impinging jet

1. Introduction

Air curtains (ACs) are plane turbulent impinging jets that are used to separate two environments in terms of heat and mass transfer while still allowing traffic between these environments. They can be implemented at the entrance of commercial, institutional and industrial buildings in view of indoor air quality, thermal comfort and energy efficiency (Eurovent, 2016; ASHRAE, 2019a;b). However, the range of applications for air curtains extends beyond building entrances to, for example, the healthcare, food processing, chemical, fire safety, and mining industries. ACs are used to avoid heat losses from indoor to

outdoor environments, to maintain adequate indoor air quality conditions in clean rooms and operating theaters (Shih et al., 2011; Zhai and Osborne, 2013), to retain low temperatures and cooling properties in cold storage and refrigerating rooms (Foster et al., 2006; Gil-Lopez et al., 2014; Giraldéz et al., 2016), to restrain air pollutant dispersion or heat losses in industrial processes (Popendorf, 2006; Trinks et al., 2007) and to limit the spread of particles and smoke in excavation zones or during fire incidents (Gupta et al., 2007; Luo et al., 2013; Krajewski, 2013; Nie et al., 2016; Wang et al., 2018). Their numerous applications have long motivated a general interest in adequately evaluating and improving their performance.

The AC technology was successfully incorporated in the built environment in 1952 (Norton, 1959; Etkin and Goering, 1971). Nevertheless, it was only until a decade later that early studies addressing AC performance emerged (e.g. Sleight, 1961; Hetstroni et al., 1963; Takahashi and Inoh, 1965; Hayes and Stoecker, 1969a,b). Hayes and Stoecker (1969a,b) pioneered the development of an analytical model to characterize an AC system in a perfectly sealed (airtight) room. This characterization was based on the stability of the jet by means of the dimensionless parameter known as the 'deflection modulus' D_m. This modulus was defined as the ratio of the jet momentum flux M_{jet} and the stack pressure load ΔP caused by air density variations in the absence of other external pressure forces (e.g. wind effects, room pressurization):

$$D_m = \frac{M_{jet}}{\Delta P} = \frac{\rho_0 W_{jet} V_{jet}^2}{g h_{jet}^2 (\rho_c - \rho_w)} \qquad (1)$$

where ρ_0 is a reference density, W_{jet} the jet width and V_{jet} the jet discharge velocity, g the gravitational acceleration, h_{jet} the jet height, ρ_c the density of air on the cold side and ρ_w the density of air on the warm side of the AC. The model by Hayes and Stoecker (1969a,b) has laid the foundation for a large amount of subsequent research on the topic (e.g. Howell and Shiabata, 1980; Sirén, 2003a; Costa et al., 2006; Foster et al., 2006; Frank and Linden, 2014; 2015; Viegas and Cruz, 2018).

After the 1960s, an increasing number of studies have been conducted on AC performance. Sirén (2003a) presented three different analytical methods for dimensioning an upward-blowing AC based on momentum balances and discussed their performance in terms of the resulting axis of deflection to achieve an acceptable impact point for the AC jet. In a second paper, Sirén (2003b) focused on the heat loss that occurs through the doorway above which the AC is placed and he analytically examined a few approaches for the evaluation of the thermal performance of the system. Giráldez et al. (2013) extended the work by Sirén and proposed a semi-analytical method for dimensioning ACs with a more generally-applied downward-blowing jet using a similar consideration of the jet impact point. In addition, the authors adopted an efficiency formulation (i.e., a separation efficiency) based on heat transfer as a performance indicator to investigate the influence of different system parameters.

Regarding AC use in the refrigeration sector, Foster et al. (2006; 2007), based on earlier work on the infiltration characteristics of cold rooms with open doors (Foster et al., 2002; 2003), investigated appropriate AC jet discharge velocities and AC angles to improve the sealing of a cold room. Extensive parametric studies were also performed by Jaramillo et al. (2009), Gonçalves et al. (2012a; 2012b; 2019) and Giráldez et al. (2016). These studies calculated CO_2 concentrations, energy gains or water vapor entrainment to indicate AC performance. In most cases these quantities were incorporated into an efficiency formula (i.e., a separation efficiency).

For AC application at building entrances, Costa et al. (2006) conducted a parametric study in which the overall flow structure of an AC was described and the AC performance, using the separation efficiency based on heat transfer as indicator, was analyzed for generalized summer and winter conditions under various jet operating parameters. Wang and Zhong (2014) characterized infiltration through a door opening with an AC and presented a model to quantify this infiltration based on a modification of the well-known orifice equation applied to each of the flow regimes found in the AC (i.e., inflow breakthrough, outflow breakthrough and jet impingement condition), also taking into account door usage patterns. This investigation preceded a number of related studies (e.g. Goubran et al., 2016; 2017; Qi et al., 2018; Yang et al., 2019). Frank and Linden (2014; 2015) explored the separation efficiency as affected by multiple openings in the building envelope (Frank and Linden, 2014), as well as of positive buoyant jets originating from heated ACs (Frank and Linden, 2015).

As indicated in the above-mentioned overview of previous studies, different indicators have been used to mark the performance of ACs, including heat transfer correlations (Costa et al., 2006; Jaramillo et al., 2009; Gonçalves et al., 2012a; 2012b; 2019; Van Belleghem et al., 2012; Giraldéz et al., 2016; Moureh and Yataghene, 2016), infiltration or mass transfer correlations (Frank and Linden, 2014; Wang and Zhong, 2014; Giraldéz et al., 2016; Goubran et al., 2016; Qi et al., 2018; Yang et al., 2019), concentration distributions (Hu et al., 2008; Shih et al., 2011), temperature distributions (Yu et al., 2016; Cong et al., 2019) and jet stability parameters (Lajos and Preszler, 1975; Guyonnaud et al., 2000; Viegas and Cruz, 2018). However, the most commonly used performance indicator in both the scientific literature and the industry is the 'separation/sealing efficiency' (or 'separation effectiveness') η_s (e.g., Robertson and Shaw, 1978; Guyonnaud et al., 2000; Sirén, 2003b; Costa et al., 2006; Foster et al., 2006; 2007; Jaramillo et al., 2009; Shih et al., 2011; Gonçalves et al., 2012a; 2012b; 2019; Van Belleghem et al., 2012; Giraldez et al., 2013; 2016; Frank and Linden, 2014; 2015; Yu et al., 2016; Goubran et al., 2017; ASHRAE 2019a). This parameter is based on the heat or mass flow across an opening with AC as compared to the same opening without AC:

$$\eta_s = 1 - \frac{\dot{q}_{ac}}{\dot{q}_{ref}} \qquad (2)$$

where $\dot{q}$ denotes the energy or mass flow, and the subscripts *ac* and *ref* refer to the opening with and without the AC, respectively.

The suitability of a performance indicator depends on the particular conditions and settings of a certain AC system. The large degree of adaptability of the AC technology to different situations perhaps requires an adaptable performance indicator on the one hand, that better represents the qualities of a given system. On the other hand, a general and well-agreed upon definition is preferable over various individual definitions, in view of clarity of communication and intercomparison.

The objective of this paper therefore is to introduce a performance indicator that, defined using a conventional efficiency formula, is suitable for different types of systems that may involve different AC configurations (downward blowing, upward blowing, lateral blowing, multiple jets, etc.) at multiple scales, different transported quantities (heat, water vapor, particles, gases, etc.) subjected to various transport mechanisms (advection, molecular and turbulent diffusion) and varying environmental conditions (gradients in environmental pressure and/or density). The principle of this performance indicator is

illustrated using a generic case study, which is based on computational fluid dynamics (CFD) employing validated large eddy simulations (LES).

The paper is organized as follows. Section 2 introduces the adapted separation efficiency as the performance indicator. Section 3 presents the CFD validation study. Section 4 describes two representative AC scenarios that are employed to demonstrate the new performance indicator, and presents the computational settings and parameters used for these scenarios. In Section 5, the results from the two AC scenarios are presented with the new performance indicator. Summary and conclusions are provided in Section 6.

2. Adapted separation efficiency

Notwithstanding the numerous AC indicators proposed in the literature, no consensus exists on the consistent use of a general indicator to properly evaluate performance across a wide variety of AC systems and operating conditions. Moreover, there is still room for improvements in the formulation of existent indicators. For instance, the inapplicability of indicators based on temperature and heat flow correlations (e.g., Costa et al., 2006; Jaramillo et al., 2009; Gonçalves et al., 2012a; 2012b; 2019; Van Belleghem et al., 2012; Giraldéz et al., 2016; Moureh and Yataghene, 2016) becomes evident when dealing with isothermal or nearly isothermal situations, where these indicators are inherently not valid as heat transfer does not take place or is negligible. In a similar manner, indicators that are niche specific, such as those formulated in terms of smoke parameters (e.g., smoke-blocking performance, smoke tightness) tailored for ACs in fire safety applications (Jung et al., 2016; Viegas and Cruz, 2018), are not very suitable for different situations. Indicators that characterize AC jet stability (e.g., Lajos and Preszler, 1975; Guyonnaud et al., 2000; Viegas and Cruz, 2018) can be applied to a wide range of situations, however, they do not provide information on the transport of heat or mass between the environments separated by the AC. Lastly, indicators formulated in terms of mass transfer (e.g., Frank and Linden, 2014; Wang and Zhong, 2014; Goubran et al., 2016; Qi et al., 2018; Yang et al., 2019) offer a certain degree of universality since AC systems always involve mass transport. Nevertheless, until now, indicators of this type considered the global mass flow rate between the environments separated by the AC without accounting individually for bidirectional mass transport, which has two disadvantages: (1) inefficiencies related to the exchange of mass (infiltration and exfiltration occurring simultaneously where net mass balance yields zero) are neglected, and (2) the individual contribution of the mass transport in one direction cannot be isolated. The former implies that for applications in which transport of mass in both directions is important, efficiency can be to some extent miscalculated, whereas the latter suggests that for certain AC applications in which mass transport in one direction is more important than in the other direction, the use of such indicators may not be convenient. To address these limitations and to provide a widely-applicable performance indicator suitable for different types of AC systems and operating conditions, the ‘adapted separation efficiency’ indicator is proposed.

In this paper, the general definition of the separation efficiency (Eq. 2) is expanded in order to distinguish between air infiltration and exfiltration, and to consider their respective contributions to this indicator. Air infiltration refers to the transport of air from outside to within the room where the temperature or concentration needs to be guarded by the AC. Air exfiltration refers to the transport of air from inside to outside. Thereby, two distinct definitions of the separation efficiency are introduced: (1) a separation efficiency based solely on infiltration ($\eta_{s,inf}$), and (2) an adapted separation efficiency based on both infiltration and exfiltration ($\eta_{s,tot}$). This distinction is made in view of different AC applications in different

industries. On the one hand, there are applications for which infiltration is the most critical (detrimental) factor. This encompasses applications such as the confinement of smoke during fire events, which is relevant for the fire protection industry (e.g., Luo et al., 2013; Krajewski, 2013); the impediment of pollutant transport towards clean rooms or operating rooms, which is relevant for the micro-nano manufacturing and the healthcare industry (e.g., Shih et al., 2011; Zhai and Osborne, 2013); the generation of an anti-insect barrier to prevent the spread of vector-borne diseases, which is relevant for the pest control industry (e.g., Kairo et al., 2018); the containment of hazardous gases and fumes in chemical storage or process rooms, which is relevant for the chemical industry (e.g., Etkin and McKinney, 1992; Huang et al., 2007); and the restriction of dust and particle dispersion in mineral extraction and processing sites, which is relevant for the mining industry (e.g., Nie et al., 2016; Wang et al., 2018). Commercial and light-industrial building applications in the sole interest of thermal comfort and indoor air quality may also fall into this category. On the other hand, there are other common applications for which both infiltration and exfiltration are equally crucial factors affecting the performance. The most noted examples of the latter are refrigeration applications and building entrance applications, in which not only heat loss or gain due to infiltration of unconditioned air is important but also heat loss or gain due to exfiltration of already conditioned air. To ensure a consistent comparison of the AC performance under isothermal and non-isothermal environmental conditions and in order to provide a consistent performance indicator throughout, the adopted definitions of the separation efficiency are formulated based on mass transfer. This allows universal applicability of the performance indicator; i.e. not only to cases involving heat transport across an opening due to thermal effects (cross-jet temperature gradients) but also to all sorts of cases that do not involve heat transport but, for example, transport of mass due to concentration differences (e.g., cross-jet density gradients as a result of pollutant/water vapor concentration) and/or transport due to other advection/diffusion mechanisms (e.g., forced convection, pressure-driven flow). The separation efficiency based solely on infiltration ($\eta_{s,inf}$) and the separation efficiency based on both infiltration and exfiltration ($\eta_{s,tot}$) are defined as:

$$\eta_{s,inf} = 1 - \frac{\dot{m}_{in,ac}}{\dot{m}_{in,ref}} \qquad (3)$$

$$\eta_{s,tot} = 1 - \frac{\dot{m}_{in,ac}+\dot{m}_{ex,ac}}{\dot{m}_{in,ref}+\dot{m}_{ex,ref}} \qquad (4)$$

where $\dot{m}$ refers to the mass transfer rate of air (or a given gas mixture) across an opening. In the context of a building entrance, subscript 'in' relates to the transport of unconditioned air to the conditioned side (i.e., infiltration) and '*ex*' relates to the transport of conditioned air to the unconditioned side (i.e., exfiltration). Furthermore, the subscripts '*ac*' and '*ref*' are associated to the building entrance with an AC and to the corresponding reference scenario of the entrance without an AC, respectively. The mass flow rates of conditioned and unconditioned air across an opening can be calculated using the following equation:

$$\dot{m}_i = \int x_i \rho (\vec{v} \cdot \vec{n}) dA \qquad (5)$$

where x_i is the mass fraction of conditioned or unconditioned air, ρ is the average gas mixture density, $\vec{v}$ is the local velocity vector and dA is the area element of a measurement plane or surface with $\vec{n}$ its outward normal vector. The area of the measurement surface over which the integration is to be taken must encompass the full extent of the opening and this must be placed at a distance away from the AC to limit

the local influence of its flow. When solving numerically for the species conservation/transport equation, the mass fractions of unconditioned and conditioned air can be retrieved directly from a CFD solution. These mass fractions can also be derived from concentration measurements obtained experimentally. A representation of the given definitions for the situation under analysis is provided in **Figure 1**.

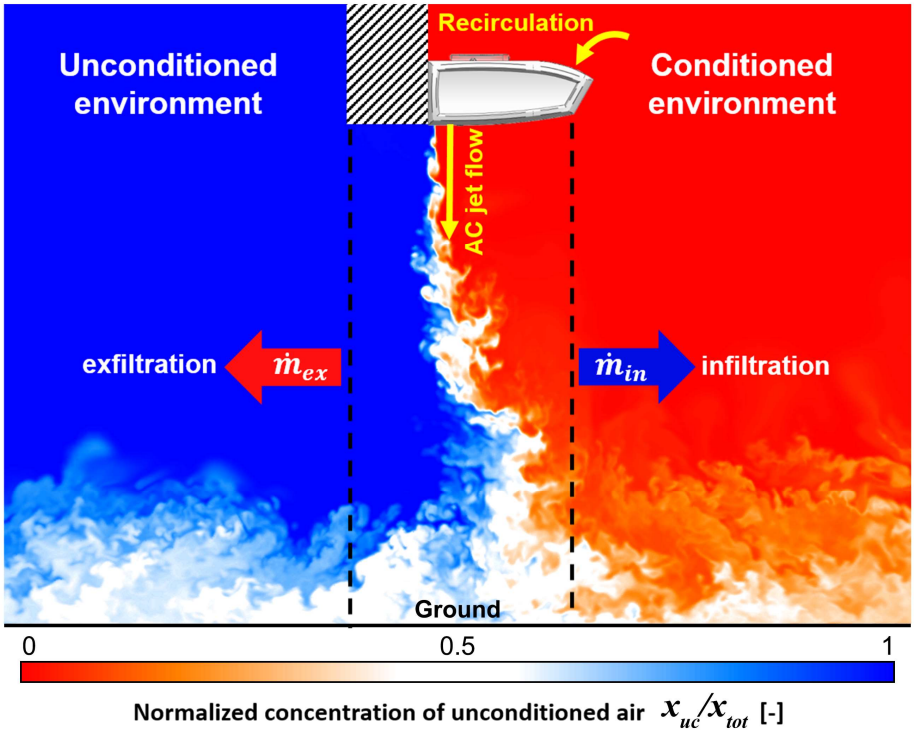

Figure 1 Illustration of the setup used for the determination of the separation efficiencies based on mass flow rates $\dot{m}$, where subscripts 'in' and 'ex' refer to infiltration and exfiltration, respectively. The dashed black lines denote measurement planes along which mass flow rates can be computed.

3. CFD validation

3.1 Experimental data

Dedicated experimental data of a generic plane impinging jet flow by Khayrullina et al. (2017) are used for the validation of the CFD simulations. The experiments were performed at reduced scale in a water tank at jet Reynolds numbers ($Re_{jet} = V_0 W_{jet}/\nu$; with V_0 the mean jet discharge velocity and ν the kinematic viscosity of the fluid) and jet height-to-width ratios ($\gamma = h_{jet}/W_{jet}$) representative of commercial ACs used at building entrances (i.e., $7{,}200 \leq Re_{jet} \leq 13{,}500$ and $22.5 \leq \gamma \leq 45$). Dynamic similarity was applied to ensure validity of the results at full scale with air as medium. This validation study employs the data corresponding to $Re_{jet} = 13{,}500$ and $\gamma = 45$. The dimensions of the water tank, as indicated in **Figure 2a**, are 360 × 2000 × 300 mm^3 (H × L × D), where the height of the tank is equivalent to h_{jet}. The water jet is issued downwards from a smoothly-shaped contraction nozzle with a discharge width of 8 mm (W_{jet}) at $V_0 = 1.69$ m/s. At the

extremities of the tank, small outlet valves are located from where the fluid leaves the tank. The complete system is under constant density conditions. Instantaneous velocity fields were measured based on particle image velocimetry (PIV) in a 2D vertical centerplane encompassing the free jet and impingement region of the flow. Polyamide particles were seeded in the conditioning section of the jet nozzle and illuminated by a light sheet powered by a dual-pulse Nd:YAG laser. Images of the particle displacement were captured by a charge-coupled device (CCD) camera in interrogation windows with span $\Delta y = 1.6\times10^{-3}$ m in the vertical (jet streamwise) direction and $\Delta x = 8\times10^{-4}$ m in the horizontal direction. The sampling frequency of image pairs for computing displacement vectors was set to 15 Hz as per the repetition rate of the laser and 5,000 uncorrelated samples were taken.

3.2 Computational settings and parameters

3.2.1 Domain and grid

The CFD simulations are performed at reduced scale with water as medium. The geometric details of the water tank and the contraction nozzle are explicitly replicated in a 3D computational domain, however, the conditioning section of the nozzle that consists of screens and a honeycomb is excluded. A high-quality computational grid suitable for LES is constructed according to best practices (e.g., Versteeg and Malalasekera, 2007; Meyers et al., 2008; Geordiadis et al., 2009; Menter, 2015). **Figure 2b-e** shows the grid over some of the surfaces of the computational domain. It is a non-conformal hybrid grid composed of an orthogonal array of cubic cells (aspect ratio = 1) for the sections encompassing the complete water tank and the bottom of the nozzle contraction, and an array of body-fitted structured hexahedral cells with low aspect ratio for the curved top of the nozzle contraction. The grid in the free-shear jet and impingement regions is especially refined on the basis of significant vorticity magnitude ($|\omega| > 20$ s^{-1}) stemming from observations in preliminary simulations. In **Figure 2b**, important turbulent flow structures originating in the jet region (Q-criterion > 4,000 s^{-2}; where $Q = \frac{1}{4}\left(\vec{\omega}^2 - 2S_{ij}S_{ij}\right)$ with S_{ij} the mean strain rate tensor) colored with vorticity magnitude are visualized. The grid is especially refined in the near-wall region of the nozzle contraction section upstream of the jet because smaller eddies dominate in this region and the conditions in this region can become particularly relevant for defining the jet discharge. Therefore, 36 cubic cells are constructed across the 8 mm contraction, yielding a dimensionless wall distance $y^* \approx 10$. The computational grid is made up of 16.8 million cells. To verify the suitability of this grid resolution, the LES index of resolution quality (LES_IQ$_v$) by Celic et al. (2005) is calculated. The LES_IQ$_v$ values for the implemented grid ranges between 74 and 95%, with an average of 87%, for the combined jet and impingement regions. An LES_IQ$_v$ value of 75% to 85% is deemed adequate for most applications where high Reynolds numbers occur (e.g. Celik et al., 2005; 2006; Klein et al. 2008).

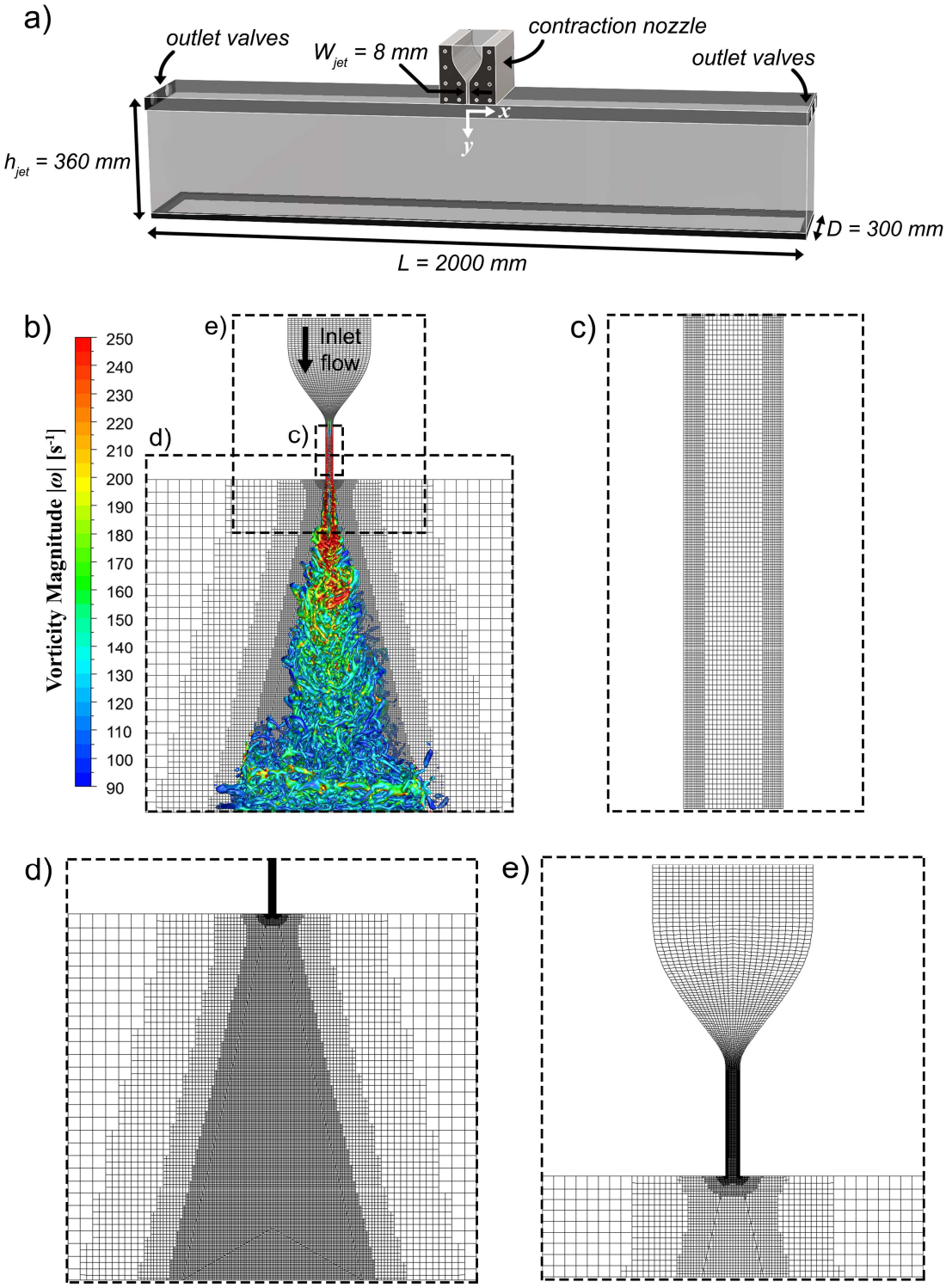

Figure 2 (a) Geometry of the water tank. (b-e) Computational grid in a vertical center plane (z/D = 0.5) of the water tank: (b) Turbulent flow structures (Q-criterion > 4,000 s^{-2}) colored by vorticity magnitude illustrating the free jet region and indicating the zone of higher grid resolution. (c-e) Close-up view of the grid.

3.2.2 Boundary conditions

A uniform streamwise velocity = 0.14 m/s, a turbulence intensity TI = 7% and a turbulence length scale l = 0.426 mm (as per the gap width of the screens in the conditioning section) are imposed in the contraction nozzle. On top of that, random time-dependent velocity perturbations are enforced by means of a fluctuating vorticity field (i.e., vortex method; Sergent, 2002). These inlet conditions yield a mean jet inlet velocity $V_0 \approx 1.7$ m/s and $TI < 0.3\%$ at the discharge opening, which is in agreement with the experiments. Outlet boundaries with zero static gauge pressure are applied at the location of the outlet valves. The remaining walls are smooth no-slip wall boundaries with a sand-grain roughness height k_s = 0 m and a roughness constant C_s = 0.5.

3.2.3 Solver settings

LES are performed using the CFD code ANSYS Fluent 18.2 (ANSYS Inc., 2017). Closure of the filtered form of the Navier-Stokes equations used in this approach is given by the wall-adapting local eddy-viscosity (WALE) sub-grid scale (SGS) model (Nicoud and Ducros, 1999). The near-wall treatment proposed by Werner and Wengle (1991) is adopted. The combination of the WALE SGS and the Werner-Wengle near-wall approximation has been successfully tested and implemented in the past for the simulation of wall-bounded constriction flows (Temmerman et al., 2003). Such type of flow is also present at the contraction section in this study, at which the grid resolution is critical to determine the correct jet discharge profiles. The pressure-velocity coupling is carried out by means of the pressure implicit with splitting of operators (PISO) method (Issa, 1986). Second-order accurate schemes are employed for the discretization of the spatial and temporal terms of the flow equations: bounded central differencing for the momentum equation, central differencing for the pressure equation and bounded second-order implicit for time integration. Discretization in time satisfies the Courant-Friedrichs-Lewy (CFL) condition ($CFL \leq 1$; stability condition) throughout the domain with a time step size Δt = 0.0001 s. The flow is initialized with 16 flow-through times (from the jet discharge to the impingement surface) and data sampling is performed for 30 flow-through times.

3.3 Results and validation

In **Figure 3**, LES simulation results are compared to the experimental data in terms of the dimensionless mean (time-averaged) velocity magnitude $|V|/V_0$. The comparison is made along the jet centerline ($x/w_{jet} = 0$, $z/D = 0.5$) and a cross-jet line ($y/h_{jet} = 0.5$, $z/D = 0.5$), since velocity measurements at these positions provide information on the decay and spread of the jet, respectively. In general, the simulation results exhibit a good agreement with the experiments. Along the jet centerline the normalized root-mean-square error (NRMSE) is 4.6% and the mean correlation (Pearson's factor) is 99.4%. The agreement is marginally lower for the cross-jet line with a NRMSE of 7.6% and a mean correlation of 98.5% as a result of the slightly higher jet spread predicted at mid height (see **Figure 3b**). Nonetheless, the deviations are considered to be well within reasonable limits. Therefore, the computational settings and parameters used in the validation study are deemed appropriate for the subsequent LES simulations. Note that Khayrullina et al. (2019) performed a similar validation study using steady RANS simulations that showed a similar performance to that presented here for LES: their mean correlation factors (Pearson's) vary from 96.0% to 98.0%, depending on the employed turbulence model, with an overall performance of 96.3% for both centerline and cross-jet distributions of velocity.

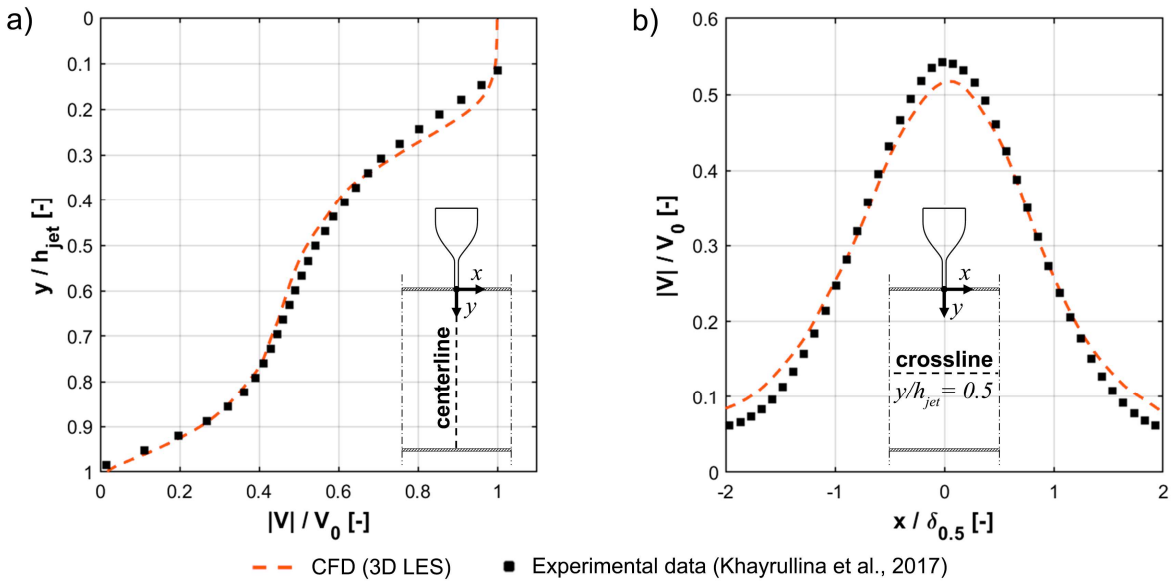

Figure 3 Comparison of LES simulations with experimental data (Khayrullina et al., 2017) in terms of the dimensionless mean velocity magnitude ($|V|/V_0$) along (a) the jet centerline ($x/w_{jet} = 0$, $z/D = 0.5$) and (b) the mid-height jet crossline ($y/h_{jet} = 0.5$, $z/D = 0.5$).

4. Test simulations

4.1 Description of test configurations

A test geometry is considered where the domain includes an AC system at the entrance of an enclosure, as in the case of a building entrance. As displayed in **Figure 4a**, this domain consists of two regions: (1) the conditioned region in the enclosure (3,500 mm height) and an opening on the right-hand side where boundary conditions of the conditioned environment are set; and (2) the unconditioned region bounded by openings on the top and left-hand side where boundary conditions of the unconditioned environment are set. The regions are separated by a thin wall where an AC device is mounted at a height of 2,200 mm above the ground. Moreover, both regions extend 6,500 mm in the lateral (x) direction from the AC discharge to allow the development of the jet flow. The domain extends 500 mm in the transversal (z) direction.

The vast majority of AC systems cope with either cross-jet air density gradients (due to differences in temperature and/or concentration of species between the separated environments) or cross-jet pressure gradients (due to forces external to the system, e.g., wind loads, room pressurization); or sometimes a combination of both (e.g., ACs at building entrances). These two frequent scenarios are independently considered in the tests of the adapted separation efficiency in this paper.

For the first scenario, a cross-jet air density difference $\Delta\rho = 0.075$ kg/m^3 is assumed. This is in line with the air density differences commonly found in AC systems for cold storage rooms, i.e. density differences resulting from air at 4°C (65% RH), as per regulations of cold storage rooms in food processing and pharmaceutics (EU Commission, 2004a;b), and air at 21°C (40% RH), which can be an expected condition for the surrounding environment. Moreover, such air temperature (and humidity) differences are

found between indoor and outdoor environments separated by ACs in moderate and cold climates during the heating season.

For the second scenario, a cross-jet air pressure difference of ΔP = 2.5 Pa is assumed, which corresponds to the recommended minimum space pressurization to restrict air pollution transport to clean areas (Streifel, 2000; AIA, 2001) as well as to reduce air infiltration through the envelope of buildings (ASHRAE, 2019a).

The range of jet momentum fluxes (M_{jet}) that are taken for the analysis extends from 2 to 6 kg/s^2 in steps of 1 kg/s^2 for the first scenario, and from 4 to 10 kg/s^2 in steps of 1.5 kg/s^2 for the second scenario. In order to calculate the adapted separation efficiency, a reference configuration with no AC (i.e., M_{jet} = 0 kg/s^2) is calculated for each scenario.

4.2 Computational settings and parameters

4.2.1 Domain and grid

The computational domain is as outlined in subsection 4.1 and demonstrated in Figure 4. Various computational grids are created for this domain in order to capture the distinct flow regimes of the AC, as shown in **Figure 4b-d**. The grids are created based on similar acceptance criteria as for the grid in the validation study. The grids are primarily made of prismatic cells with aspect ratios close to unity. Sub-domains with non-conformal interfaces (ratio 2:1) are created to further refine the grids in turbulent flow regions of critical importance, characterized by high levels of vorticity and where Q-criterion is significant (see e.g., **Figure 4b-d**). The grid resolution (with cell size Δ) is determined by an a priori approximate calculation of the integral length scale of turbulence (l_0) and subsequently enforcing the relation $l_0/\Delta \geq 12.5$ throughout important flow regions of the domain, except for the potential core region of the jet where $l_0/\Delta \approx 4.8$ is implemented. These relations, as recommended by Gerasimov (2016), are conservative estimates to determine the grid resolution in order to resolve 80 to 90% of the turbulent kinetic energy based on Kolmogorov's -5/3 spectrum. The total number of cells in the grids varies from 18.4 to 22.1 million for the different scenarios (AC in operation) and 18.9 million for their reference configurations (AC inactive).

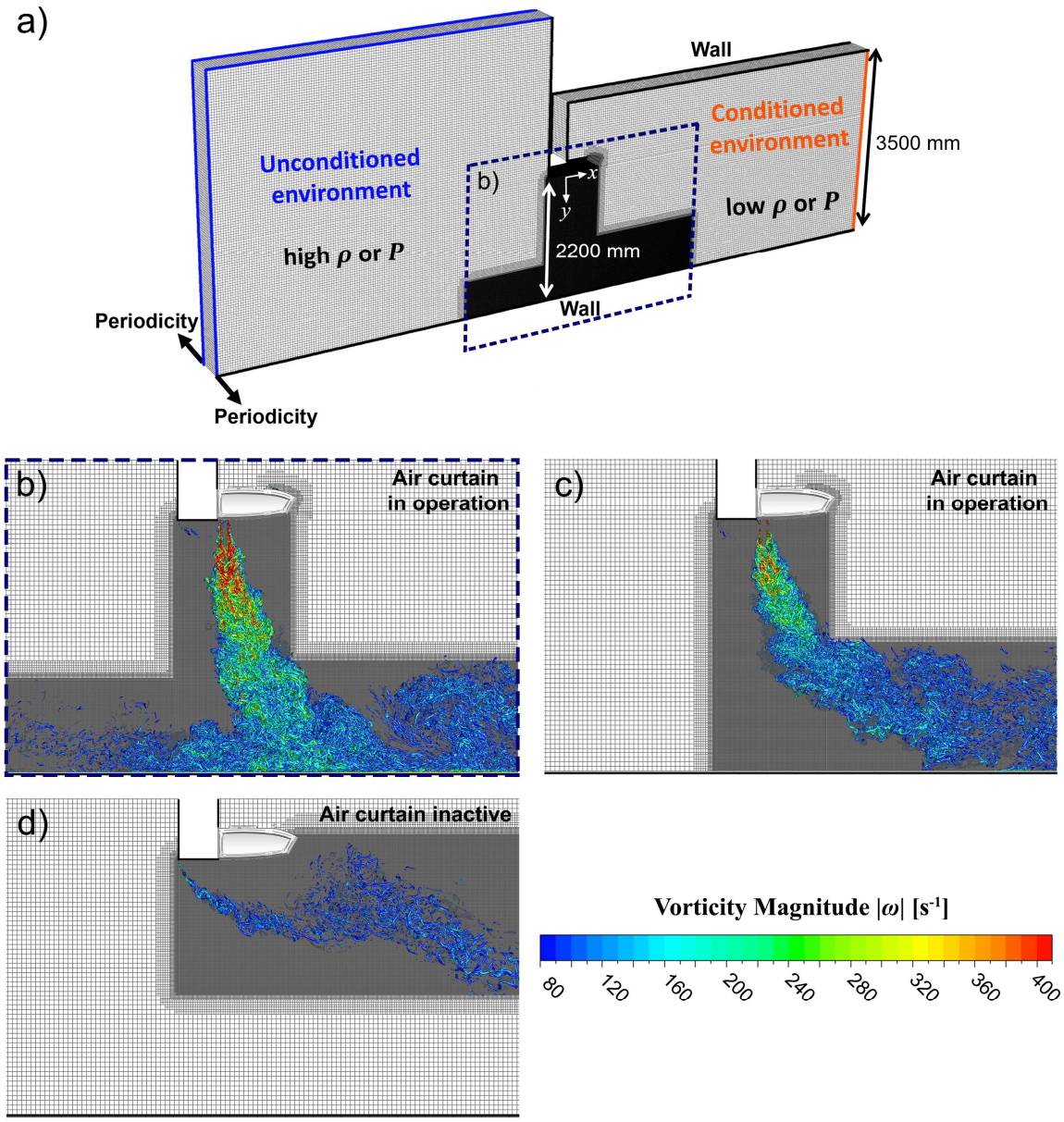

Figure 4 (a) Computational domain and grid visualization over its surfaces. The bold black lines indicate wall boundaries whereas bold blue and orange lines indicate the boundaries of the unconditioned and conditioned environment, respectively, where differences in density or pressure are imposed. (b-d) Grid configurations corresponding to different flow regimes and enlarged view of zones with higher grid resolution where the formation of important vortical structures (Q-criterion > 4,000 s^{-2}) is anticipated. Colors indicate values of the vorticity magnitude. Note that in (d) the AC is inactive and the vorticity depicted is generated by the velocity gradients due to separation of the incoming flow.

4.2.2 Boundary conditions and fluid/flow properties

At the inlet (discharge) of the AC device, a uniform mean velocity normal to the boundary is imposed in agreement with the jet momentum flux of the respective configuration (see **Section 4.1**). The width of the discharge nozzle is W_{jet} = 65 mm in all configurations. The vortex method is used to generate random time-dependent fluctuations of the velocity at the inlet. Turbulence intensity is specified as TI = 6% (as a typical value for ACs; Field and Loth, 2004) along with a turbulence length scale l = 4.26 mm, which is based on the spacing of the discharge flow rectifier of a commercial AC (Biddle B.V., 2016). The air flow rate supplied by the AC at the discharge is equal to the rate extracted by the AC (recirculation), hence consistent with mass conservation. Because the analysis is intended to be independent of the length (in z direction) of a certain AC, periodicity is enforced in the transversal direction.

A mixture of two distinct air species is used to differentiate between 'conditioned' and 'unconditioned' air. These air species have the same physical properties; except for density for the first scenario, which differs in accordance with the conditions outlined in **Subsection 3.2**. The density in the air mixture is computed from a volume-weighted mixing-law. At the corresponding openings of the conditioned and unconditioned regions, boundary conditions are specified in terms of pressure and backflow concentration. Whereas a static gauge pressure of zero is prescribed at all openings, a static gauge pressure of 2.5 Pa is enforced at the unconditioned side in the second scenario, in order to generate a pressure gradient to drive the flow. Backflow concentration at these boundaries is consistent with the denomination of the respective region (i.e., conditioned or unconditioned). Lastly, solid surfaces of the domain in contact with the gas mixture are all no-slip walls with k_s = 0 m and C_s = 0.5. The mentioned boundary conditions are shown in **Figure 5**.

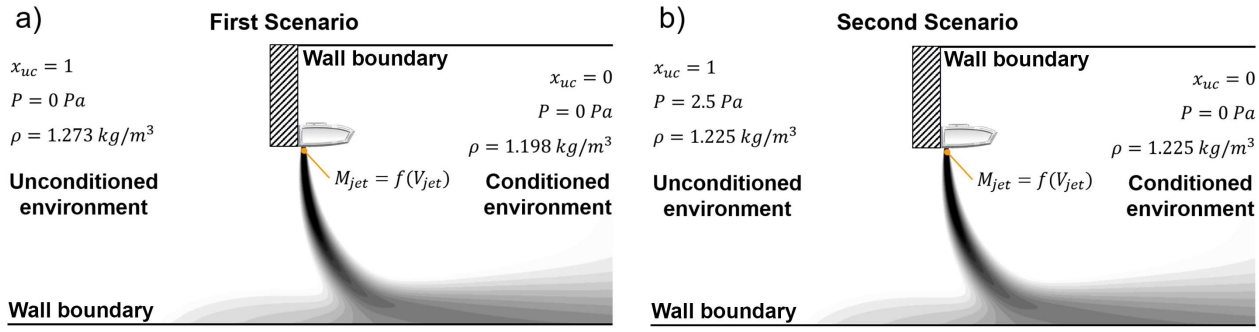

Figure 5 Indication of boundary conditions for test simulations: (a) first scenario (density difference) and (b) second scenario (pressure difference).

4.2.3 Solver settings

The solver settings are based on the validation study in **Section 3**. LES simulations are performed in combination with the WALE SGS model (Nicoud and Ducros, 1999) and the Werner-Wengle model (Werner and Wengle, 1991) for near-wall treatment. The PISO algorithm (Issa, 1986) is adopted for pressure-velocity coupling. Bounded central differencing for the momentum equation, second-order upwind for species transport and second-order implicit for the transient formulation are used. In addition, pressure interpolation is second order. CFL ≤ 1 is ensured in the entire domain for every simulated case.

The turbulent Schmidt number Sc_t is taken equal to 0.7 in this study, as recommended for jet flows (e.g. Yimer et al., 2002; Tominaga and Stathopoulos, 2007; ANSYS Inc., 2017).

4.2.4 Estimation of mass flow rates

To quantify the mass flow rates needed in **Equations 3 and 4**, two measurement planes are used. One at the conditioned side to calculate the infiltration of unconditioned air, and another at the unconditioned side to calculate the exfiltration of conditioned air (Figure 1). The location of the measurement planes in the CFD model is based on a sensitivity analysis and is taken sufficiently far away from the AC in order to avoid too strong local influences of the AC flow. For the present analysis, the distance of the measurement planes from the AC is determined to be 1,000 mm. In view of the transient simulations, the instantaneous mass flow rates are averaged over a flow time of 10 seconds once a stationary (i.e. statistically steady) condition is reached.

5. Results

Figure 6 shows time-averaged contours of mass fractions of unconditioned air (X_{uc}/X_{tot}), revealing typical flow regimes of the AC system, which are present for both scenarios (density gradients and pressure gradients). From left to right, these are (1) the reference configuration (no AC; Figure 6a); (2) breakthrough with excessive infiltration (Figure 6b): (3) optimum jet impingement condition (Figure 6c); (4) jet impingement with excessive exfiltration (Figure 6d). Note that two major mechanisms are involved in the transport of heat and mass between environments separated by an AC. On the one hand there is advection caused by the bulk movement of fluid driven by pressure and/or density gradients. This first mechanism of transport is clearly visible in regimes (1) and (2) (Figures 6a and b) where there is no AC at all or the AC is not sufficiently strong to entirely seal the opening, and therefore an evident stream of unconditioned air is transported to the conditioned side. On the other hand, there is entrainment and mixing of surrounding fluid that intrinsically occurs in the jet of the AC because of the turbulence that develops in its shear layer. Unconditioned fluid that entrains into the jet is carried in the stream and a portion of it is transported to the conditioned side when the jet impinges on the ground and splits, or it is transported with the jet if impingement does not occur. Regardless of the injected momentum flux by the AC, some amount of infiltration always happens via entrainment and turbulent mixing. This can be noticed more clearly for regime (4) in Figure 7, where infiltration by means of advection is fundamentally suppressed. Note that the AC does not supply unconditioned air; i.e., all unconditioned air present on the right-hand side is transported from the left-hand side through the AC. The observed flow regimes are similar to those reported before in literature (e.g., Frank and Linden, 2014; Wang and Zhong, 2014); however, it is interesting to note how those regimes are linked to significant variations in the proposed adapted separation efficiency.

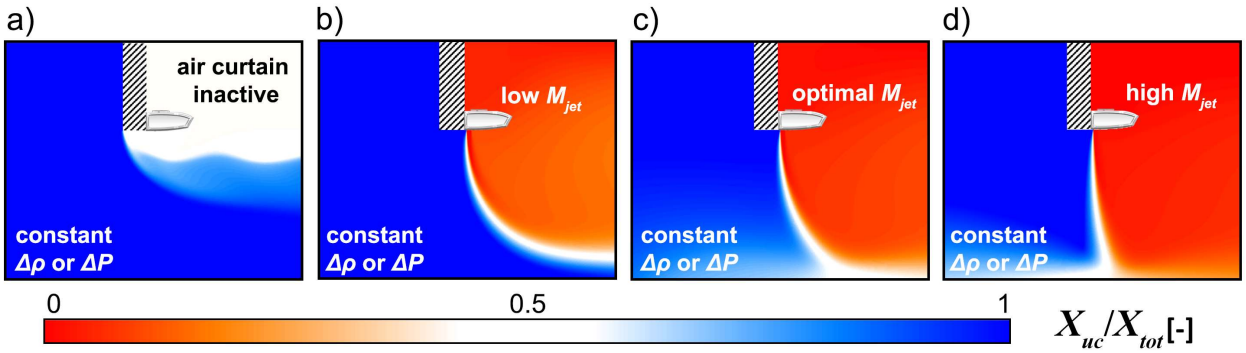

Figure 6 Contours of time-averaged unconditioned air concentration displaying the distinct flow regimes in the system: (a) air curtain inactive, (b) breakthrough with excessive infiltration, (c) optimum jet impingement condition, and (d) jet impingement with excessive exfiltration.

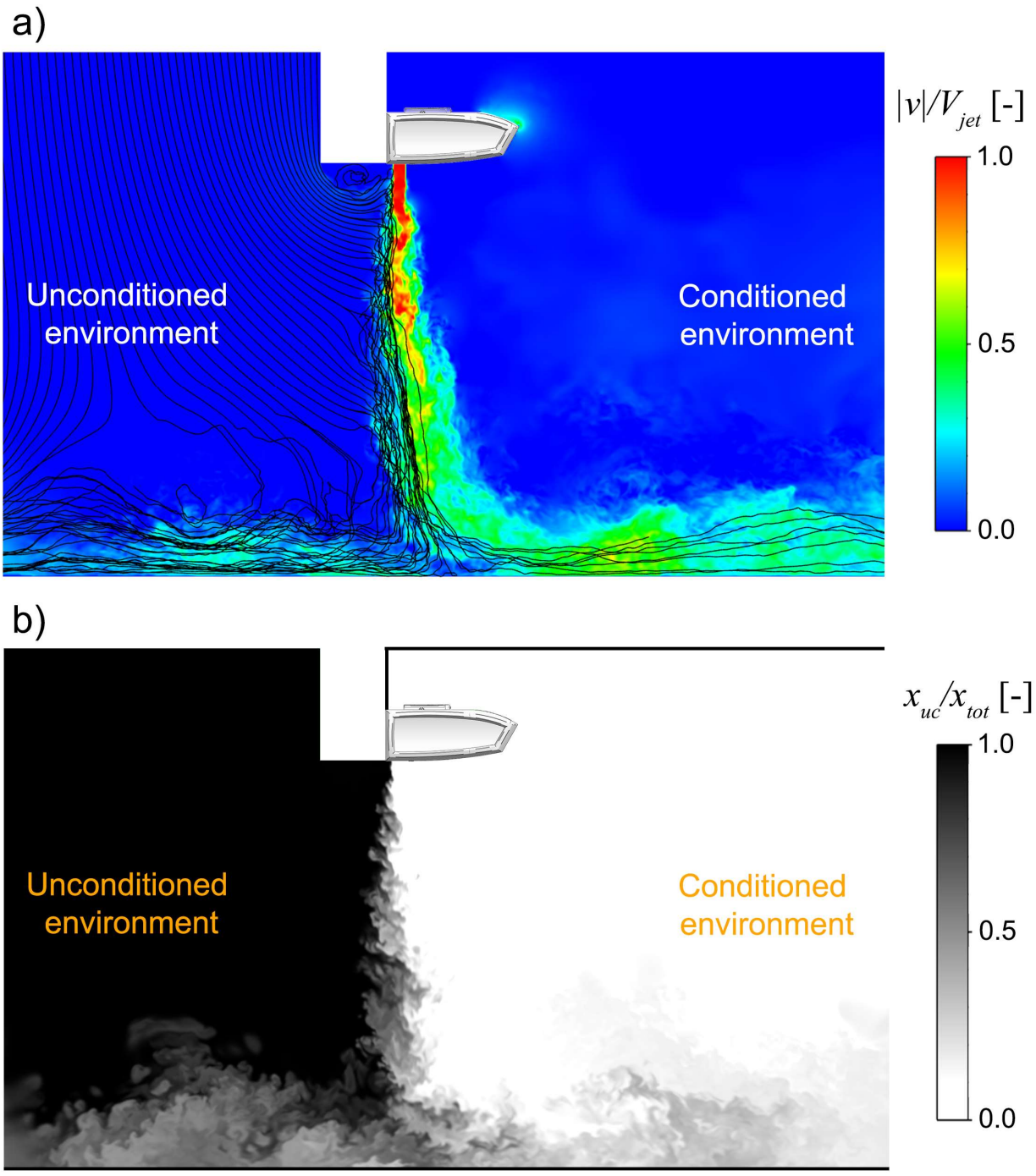

Figure 7 (a) Contours of instantaneous velocity magnitude normalized with the jet velocity and pathlines from massless particles (black lines) released at the boundary of the unconditioned environment. (b) Contours of instantaneous concentration of unconditioned air (mass fraction; x_{uc}/x_{tot}). This example pertains to an AC system with M_{jet} = 5 kg/s^2 and $\Delta\rho$ = 0.075 kg/m^3.

Figure 8 indicates different outcomes with respect to AC performance depending on how the separation efficiency is determined. For the tested configurations, the separation efficiency based solely on infiltration ($\eta_{s,inf}$) indicates increasing performance with increasing jet momentum flux. However, the separation efficiency based on both infiltration and exfiltration ($\eta_{s,tot}$) indicates an optimum jet momentum flux at approximately M_{jet} = 3 kg/s^2 ($\eta_{s,tot}$ = 0.67) and M_{jet} = 5.5 kg/s^2 ($\eta_{s,tot}$ = 0.83) for scenarios 1 (cross-jet density gradient) and 2 (cross-jet pressure gradient), respectively, after which a decreased separation efficiency for higher jet momentum fluxes is shown. The decreased separation efficiency for higher jet momentums can be attributed to the substantial exfiltration that takes place at too high jet momentum fluxes, which translates into potential inefficiencies (e.g., energy losses when the conditioned environment is purposely subjected to heating or cooling). Both efficiency indicators show similar values at lower jet momentum fluxes (when M_{jet} < 3 kg/s^2 for the first scenario and M_{jet} < 5.5 kg/s^2 for the second scenario), which is caused by the low degree of exfiltration in these situations, making infiltration dominant when calculating the separation efficiency.

For both scenarios the separation efficiency based on infiltration increases asymptotically with the jet momentum flux; its efficiency is eventually limited by the inherent entrainment and turbulent mixing processes that take place in the jet. In contrast, the separation efficiency based on both infiltration and exfiltration displays an optimum value for a certain jet momentum flux, above which the efficiency is penalized by excessive exfiltration, whereas for a lower jet momentum flux, the efficiency drops due to excessive infiltration. Consequently, the optimum separation efficiency is found when both infiltration and exfiltration are minimized. Note that in this study the optimum value of the separation efficiency is approximated from the discrete values of M_{jet} that are adopted and that additional simulations would be needed to determine the exact optimum.

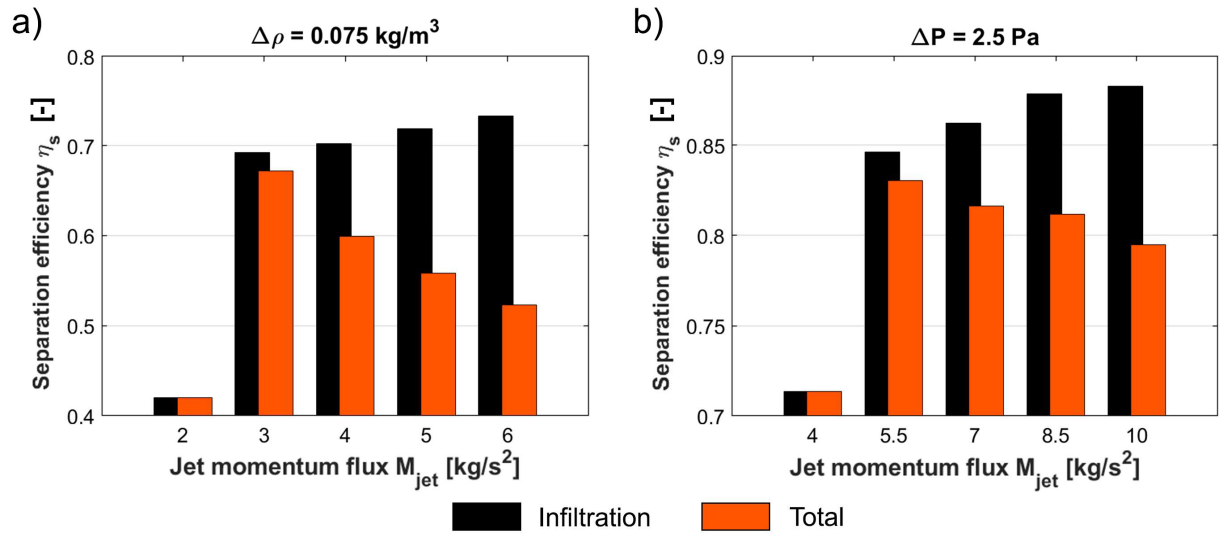

Figure 8 Variation of the adapted separation efficiency (η_s) as a function of the jet momentum flux (M_{jet}) for infiltration $\eta_{s,inf}$ (black bars) and total $\eta_{s,total}$ (red bars). (a) Cross-jet density difference ($\Delta\rho$ = 0.075 kg/m^3). (b) Cross-jet pressure difference (ΔP = 2.5 Pa).

6. Summary and conclusions

The design, analysis and optimization of an AC system requires the use of a performance indicator that is appropriate for the specific application at hand. AC applications are as varied as the industries that adopt them in their processes. Furthermore, AC systems in diverse applications are characterized by different operating conditions which in turn may involve different transport mechanisms of mass and/or energy. Such complexity and variability implies that indicators are not always suitable to determine performance of certain systems.

This paper introduces a performance indicator that conveniently aligns with the fundamental intent of the specific AC application in question, hence enabling performance assessment in different systems. The proposed "adapted separation efficiency", which is split into two indicators, has the following advantages:

- It allows to obtain a complete picture of the separation of environments by segregating the different contributions to mass transport and considering them for the calculation of the performance indicators.
- It is useful for evaluating AC performance under distinct operating conditions and involving various transport phenomena, thus being suitable for AC systems in diverse applications.
- It adopts a standardized formulation to facilitate understanding and communication of results.
- Its implementation is straightforward, especially in numerical simulations, which are commonplace for AC studies.

A demonstration of two scenarios is presented through large eddy simulations whereby the significance of using the proposed indicators is explained. This demonstration highlights the different outcomes with respect to AC performance depending on the selection of the separation efficiency indicator.

It is considered that the separation efficiency based solely on infiltration ($\eta_{s,inf}$) is more adequate for applications in which conserving the properties of the conditioned environment is the single priority. Therefore, these applications can benefit from the injection of somewhat larger jet momentum fluxes by the AC as long as the asymptotic behavior of this separation efficiency is considered when increasing the injection of momentum, which could represent a trade-off between separation efficiency and energy savings (due to reduced power consumption by the fans of the AC device). On the other hand, the separation efficiency based on both infiltration and exfiltration ($\eta_{s,tot}$) is more adequate for applications in which a complete separation between the two environments is desired in terms of temperature or concentration. For these cases, the injection of momentum by the AC would have to be optimized with respect to the cross-jet loads generated by the environmental conditions of the system in order to maximize the separation efficiency. Both too low and too high momentum fluxes would cause inefficiencies and a decreased adapted separation efficiency.

It is worth noting that the proposed indicators here are formulated in terms of (species) mass transport to ensure the applicability of the indicators in both isothermal and non-isothermal conditions of the environment surrounding the AC. For such cases, the energy and species conservation equations are analogous and take the same form, except for their different diffusivities; nevertheless, transport in AC flows is heavily dominated by advection. Notwithstanding, for some specialized applications is relatively common to find heated or cooled ACs. The latter case is unique from a physical perspective because while the species conservation equation retains the same form, the energy equation changes by incorporating a

buoyancy source term. Although the proposed indicators fully consider the exchange of mass that occurs in a system, they do not take into account that the exfiltration of heated air can entail a greater energy loss than that of non-heated air. Therefore, such particular case would benefit from an indicator formulated based on the energy balance of the system, in addition to the adapted separation efficiency that is proposed in this paper, in order to obtain a complete understanding of the performance of the system in terms of both, mass separation and energy conservation. However, for the vast majority of situations, which do not involve buoyant jets, the use of the proposed adapted separation efficiency alone is generally sufficient to adequately assess the overall performance of an AC system.

7. Acknowledgements

The Research Foundation – Flanders (FWO) is acknowledged for the financial support of the first author (project FWO G085618N). In addition, Twan van Hooff is currently a postdoctoral fellow of the Research Foundation – Flanders (FWO) and acknowledges its financial support (project FWO 12R9718N). This work was sponsored by NWO Exacte Wetenschappen (Physical Sciences) for the use of supercomputer facilities, with financial support from the Nederlandse Organisatie voor Wetenschappelijk Onderzoek (Netherlands Organization for Scientific Research, NWO). Finally, the authors gratefully acknowledge the partnership with ANSYS CFD.

8. References

AIA. (2001). *Guidelines for the design and construction of hospital and health care facilities.* American Institute of Architects.

ANSYS Inc. (2017). *ANSYS Fluent 18.2 - Theory Guide.* USA: Lebanon.

ASHRAE. (2019). *ASHRAE Handbook - HVAC Applications.* American Society of Heating, Refrigerating and Air-Conditioning Engineers.

ASHRAE. (2019). *ANSI/ASHRAE/IES Standard 90.1-2019 - Energy standard for buildings except low-rise residential buildings.* American Society of Heating, Refrigerating and Air-Conditioning Engineers.

Biddle B.V. (2016). *Personal correspondence.*

Celik, I., Cehreli, Z., & Yavruz, I. (2005). Index of resolution quality for large eddy simulations. *Journal of Fluids Engineering*, 127:949-958.

Celik, I., Klein, M., Freitag, M., & Janicka, J. (2006). Assessment measures for URANS/DES/LES: an overview with applications. *Journal of Turbulence*, 7:1-27.

Cong, L., Yu, Q., Qiao, G., Li, Y., & Ding, Y. (2019). Effects of an air curtain on the temperature distribution in refrigerated vehicles under a hot climate condition. *Journal of Thermal Science and Engineering Applications*.

Costa, J., Oliveira, L., & Silva, M. (2006). Energy savings by aerodynamic sealing with a downward-blowing plane air curtain - A numerical approach. *Energy and Buildings*, 1182 - 1193.

Etkin, B., & Goering, P. (1971). Air-curtain walls and roofs - 'Dynamic' structures. *Philosophical Transactions of the Royal Society of London. Series A, Mathematical and Physical Sciences, 269*(1199), 527-543.

Etkin, B., & McKinney, W. (1992). An air-curtain fume cabinet. *American Industrial Hygiene Association Journal, 53*(10), 625-631.

EU Commission. (2004). Regulation (EC) 852/2004 concerning the hygiene of foodstuffs. *Official Journal of the European Union*.

EU Commission. (2004). Regulation (EC) 853/2004 concerning the specific hygiene rules for food of animal origin. *Official Journal of the European Union*.

Eurovent. (2016). *Air curtains guidebook.* Brussels, Belgium: Europe's Industry Association for Indoor Climate, Process Cooling, and Food Cold Chain Technologies.

Field, B., & Loth, E. (2004). An air curtain along a wall with high inlet turbulence. *Journal of Fluids Engineering*, 391-398.

Foster, A., Barrett, R., James, S., & Swain, M. (2002). Measurement and prediction of air movement through doorways in refrigerated rooms. *International Journal of Refrigeration, 25*(8), 1102-1109.

Foster, A., Swain, M., Barrett, R., & James, S. (2003). Experimental verification of analytical and CFD predictions of infiltration through cold store entrances. *International Jorunal of Refrigeration*, 918 - 925.

Foster, A., Swain, M., Barrett, R., D'Agaro, P., & James, S. (2006). Effectiveness and optimum jet velocity for a plane jet air curtain used to restrict cold room infiltration. *International Journal of Refrigeration*, 692 - 699.

Foster, A., Swain, M., Barrett, R., D'Agaro, P., Ketteringham, L., & James, S. (2007). Three-dimensional effects of an air curtain used to restrict cold room infiltration. *Applied Mathematical Modelling*, 1109 - 1123.

Frank, D., & Linden, P. (2014). The effectiveness of an air curtain in the doorway of a ventilated building. *Journal of Fluid Mechanics*, 130 - 164.

Frank, D., & Linden, P. (2015). The effects of an opposing buoyancy force on the performance of an air curtain in the doorway of a building. *Energy and Buildings*, 20 - 29.

Geordiadis, N., Rizzetta, D., & Fureby, C. (2009). *Large-Eddy Simulations: Current Capabilities, Recommended Practices, and Future Research.* Cleveland, Ohio: NASA.

Gerasimov, A. (2016). *Quick Guide to Setting Up LES-type Simulations.* ANSYS Sweden AB.

Gil-Lopez, T., Castejon-Navas, J., Galvez-Huerta, M., & O'Donohoe, P. (2014). Energetic, environmental and economic analysis of climatic separation by means of air curtains in cold storage rooms. *Energy and Buildings, 74*, 8-16.

Giraldéz, H., Pérez Segarra, C., Oliet, C., & Oliva, A. (2016). Heat and moisture insulation by means of air curtains: Application to refrigerated chambers. *International Journal of Refrigeration*, 1 - 14.

Giraldéz, H., Pérez Segarra, C., Rodríguez, I., & Oliva, A. (2013). Improved semi-analytical method for air curtains prediction. *Energy and Buildings*, 258 - 266.

Gonçalves, J., Costa, J., & Lopes, A. (2019). Parametric study on the performance of an air curtain based on CFD simulations - New proposal for automatic operation. *Journal of Wind Engineering and Industrial Aerodynamics, 193*.

Gonçalves, J., Costa, J., Figueiredo, A., & Lopes, A. (2012). CFD modelling of aerodynamic sealing by vertical and horizontal air curtains. *Energy and Buildings*, 153 - 160.

Gonçalves, J., Costa, J., Figueiredo, A., & Lopes, A. (2012). Study of the aerodynamic sealing of a cold store – Experimental and numerical approaches. *Energy and Buildings*, 779-789.

Goubran, S., Qi, D., & Wang, L. (2017). Assessing the dynamic efficiency of air curtain in reducing whole building annual energy usage. *Building Simulation*, 497 - 507.

Goubran, S., Qi, D., Saleh, W., Wang, L., & Zmeureanu, R. (2016). Experimental study on the flow characteristics of air curtains at building entrances. *Building and Environment*, 225 - 235.

Gupta, S., Pavageau, M., & Elicer-Cortés, J. (2007). Cellular confinement of tunnel sections between two air curtains. *Building and Environment, 42*(9), 3352-3365.

Guyonnaud, L., Solliec, C., De Virel, M., & Rey, C. (2000). Design of air curtains used for air confinement in tunnels. *Experiments in Fluids*, 377 - 384.

Hayes, F., & Stoecker, W. (1969). Design data for air curtains. *ASHRAE Transactions*, 168 - 180.

Hayes, F., & Stoecker, W. (1969). Heat transfer characteristics of the air curtain. *ASHRAE Transaction*, 153 - 167.

Hetsroni, G., Hall, C., & Dhanak, A. (1963). Heat transfer properties of an air curtain. *Transactions of the American Society of Agricultural Engineers, 6*, 328-334.

Howell, R., & Shiabata, M. (1980). Optimum heat transfer through turbulent recirculated plane air curtains. *ASHRAE Transactions 86*, 188 - 200.

Hu, L., Zhou, J., Huo, R., Peng, W., & Wang, H. (2008). Confinement of fire-induced smoke and carbon monoxide transportation by air curtain in channels. *Journal of Hazardous Materials*, 327 - 334.

Huang, R., Wu, Y., Chen, H., Chen, C., Chen, C., Chang, C., & Shih, T. (2007). Development and Evaluation of an Air-Curtain Fume Cabinet with Considerations of its Aerodynamics. *The Annals of Occupational Hygiene, 51*(2), 189–206.

Issa, R. (1986). Solution of the implicitly discretised fluid flow equations by operator-splitting. *Journal of Computational Physics*, 62:40-65.

Jaramillo, J., Pérez Segarra, C., Oliva, A., & Oliet, C. (2009). Analysis of the dynamic behavior of refrigerated spaces using air curtains. *Numerical Heat Transfer, Part A: Applications*, 553 - 573.

Jung, U., Kim, S., Yang, S., Kim, J., & Choi, Y. (2016). Numerical study of air curtain systems for blocking smoke in tunnel fires. *Journal of Mechanical Science and Technology*, 4961 - 4969.

Kairo, G., Pioz, M., Tchamitchian, S., Pelissier, M., Brunet, J., & Belzunces, L. (2018). Efficiency of an air curtain as an anti-insect barrier: the honey bee as a model insect. *Pest Management Science, 74*, 2707-2715.

Khayrullina, A., van Hooff, T., Blocken, B., & van Heijst, G. (2017). PIV measurements of isothermal plane turbulent impinging jets at moderate Reynolds numbers. *Experimental Fluids*, 58:31.

Khayrullina, A., van Hooff, T., Blocken, B., & van Heijst, G. (2019). Validation of steady RANS modelling of isothermal plane turbulent impinging jets at moderate Reynolds numbers. *European Journal of Mechanics - B/Fluids*, 75:228-243.

Klein, M., Meyers, J., & Geurts, B. (2008). Assessment of LES quality measures using the error landscape approach. In J. Meyers, B. Geurts, & P. Sagaut, *ERCOFTAC Series - Quality and Reliability of Large-Eddy Simulations* (pp. 131-142). Berlin, Germany: Springer.

Krajewski, G. (2013). Efficiency of air curtains used for separating smoke free zones in case of fire. *Proceedings of BS2013: 13th conference of the International Building Performance Simulation Association.* Chambery, France.

Lajos, T., & Preszler, L. (1975). Untersuchung von Türluftschleieranlagen - Teil 2. *Heizung, Lüftung, Klimatechnick, Haustechnik, 26*, 226-235.

Luo, N., Li, A., Gao, R., Zhang, W., & Tian, Z. (2013). An experiment and simulation of smoke confinement utilizing an air curtain. *Safety Science, 59*, 10-18.

Menter, F. (2015). *Best Practice: Scale-Resolving Simulations in ANSYS CFD.* ANSYS Germany GmbH.

Meyers, J., Geurts, J., & Sagaut, P. (2008). *ERCOFTAC Series - Quality and Reliability of Large-Eddy Simulations.* Berlin, Germany: Springer.

Moureh, J., & Yataghene, M. (2016). Numerical and experimental study of airflow patterns and global exchanges through an air curtain subjected to external lateral flow. *Experimental Thermal and Fluid Science*, 308 - 323.

Nicoud, F., & Ducros, F. (1999). Subgrid-scale stress modelling based on the square of the velocity gradient tensor flow. *Turbulence and Combustion*, 62:183-200.

Nie, W., Liu, Y., & Wei, W. (2016). Effect of suppressing dust by multi-direction whirling air curtain on fully mechanized mining face. *International Journal of Mining Science and Technology, 26*(4), 629-635.

Norton, W. (1959). Where to use a curtain of air. *Consulting Engineering*, 108-113.

Popendorf, W. (2006). *Industrial Hygiene Control of Airborne Chemical Hazards.* Taylor & Francis.

Qi, D., Goubran, S., Wang, L., & Zmeureanu, R. (2018). Parametric study of air curtain door aerodynamics performance based on experiments and simulations. *Building and Environment*, 65 - 73.

Robertson, P., & Shaw, B. (1978). The linear air curtain as a particulate barrier. *Journal of Environmental Science*, 32 - 33.

Sergent, E. (2002). *Vers une méthodologie de couplage entre la simulation des grandes échelles et les modèles statistiques.* Lyon, France: PhD Thesis. L'Ecole Centrale de Lyon.

Shih, Y., Yang, A., & Lu, C. (2011). Using air curtain to control pollutant spreading for emergency management in a cleanroom. *Building and Environment*, 1101 - 1114.

Sirén, K. (2003). Technical dimensioning of a vertically upwards blowing air curtain—part I. *Energy and Buildings, 35*(7), 681-695.

Sirén, K. (2003). Technical dimensioning of a vertically upwards-blowing air curtain—part II. *Energy and Buildings, 35*(7), 697-705.

Sleight, P. (1961). Curtains of air. *Compressed Air Magazine*, 15-17.

Streifel, A. (2000). Health-care IAQ: guidance for infection control. *Heating, Piping, Air Conditioning Engineering*, 72:28-36.

Takahashi, K., & Inoh, M. (1965). Some measurements on air Curtain efficiency for cold rooms: Quelques mesures de l'efficacité des rideaux d'air pour les chambres froides. *Proceedings of the XIth International Congress of Refrigeration 1963.* Munich, Germany.

Temmerman, L., Leschziner, M., Mellen, C., & Fröhlich, J. (2003). Investigation of wall-function approximations and subgrid-scale models in large eddy simulation of separated flow in a channel with streamwise periodic constrictions. *International Journal of Heat and Fluid Flow*, 24:157-180.

Tominaga, Y., & Stathopoulos, T. (2007). Turbulent Schmidt numbers for CFD analysis with various types of flowfield. *Atmospheric Environment*, 8091-8099.

Trinks, W., Mawhinney, M., Shannon, R., Reed, R., & Garvey, J. (2007). *Industrial furnaces.* Wiley.

Van Belleghem, M., Verhaeghe, G., T'Joen, C., Huisseune, H., De Jaeger, P., & De Paepe, M. (2012). Heat transfer through vertically downward-blowing single-jet air curtains for cold rooms. *Heat Transfer Engineering*, 1196 - 1206.

Versteeg, H., & Malalasekera, W. (2007). *An introduction to computational fluid dynamics: The finite volume method.* Glasgow, UK: Pearson Prentice Hall.

Viegas, J., & Cruz, H. (2019). Air curtains combined with smoke exhaust for smoke control in case of fire: Full-size experiments. *Fire Technology*, 211 - 232.

Wang, H., Nie, W., Cheng, W., Liu, Q., & Jin, H. (2018). Effects of air volume ratio parameters on air curtain dust suppression in a rock tunnel's fully-mechanized working face. *Advanced Powder Technology, 29*(2), 230-244.

Wang, L., & Zhong, Z. (2014). An approach to determine infiltration characteristics of building entrance equipped with air curtains. *Energy and Buildings*, 312 - 320.

Werner, H., & Wengle, H. (1991). Large-eddy simulation of turbulent flow over and around a cube in a plate channel. *8th Symposium on Turbulent Shear Flows*, (pp. 155-168). Munich, Germany.

Yang, S., Alrawashdeh, H., Zhang, C., Qi, D., Wang, L., & Stathopoulos, T. (2019). Wind effects on air curtain performance at building entrances. *Building and Environment*, 75 - 87.

Yimer, I., Campbell, I., & Jiang, L. (2002). Estimation of the turbulent Schmidt number from experimental profiles of axial velocity and concentration for high-Reynolds-number jet flows. *Canadian Aeronautics and Space Journal*, 48:195-200.

Yu, L., Beji, T., Zadeh, S., Liu, F., & Merci, B. (2016). Simulations of smoke flow fields in a wind tunnel under the effect of an air curtain for smoke confinement. *Fire Technology*, 2007 - 2026.

Zhai, Z., & Osborne, A. (2013). Simulation-based feasibility study of improved air conditioning systems for hospital operating rooms. *Frontiers of Architectural Research, 2*(4), 468-475.